Relaxation Properties of Porphyrin, Diprotonated Porphyrin, and Isoelectronic Tetraoxaporphyrin Dication in the S_2 State

Agnese Marcelli

Laboratorio Europeo di Spettroscopie non Lineari (LENS), Universitá di Firenze, via N. Carrara 1, 50019 Sesto Fiorentino, Firenze, Italy

Paolo Foggi[†]

Dipartimento di Chimica, Universitá di Perugia, via Elce di Sotto 8, 06123 Perugia, Italy

Laura Moroni, Cristina Gellini, and Pier Remigio Salvi*

Dipartimento di Chimica, Universitá di Firenze, via della Lastruccia 3, 50019 Sesto Fiorentino, Firenze, Italy

Ivana Jelovica Badovinac

Faculty of Arts and Sciences, Physics Department, University of Rijeka, Omladinska 14, Rijeka, Croatia

Received: December 18, 2006; In Final Form: January 25, 2007

The fluorescence spectra of unsubstituted porphyrin (H_2P), diprotonated porphyrin (H_4P^{2+}), and isoelectronic tetraoxaporphyrin dication ($TOxP^{2+}$) have been measured in solution at room temperature. The $S_2 \rightarrow S_0$ fluorescence has been observed, much more intense for $TOxP^{2+}$ than for H_4P^{2+} and H_2P. In the $TOxP^{2+}$ case, the $S_2 \rightarrow S_0$ fluorescence spectrum is remarkably sharp and shows an excellent mirror symmetry with respect to $S_0 \rightarrow S_2$ absorption. On the contrary, the spectra of H_4P^{2+} and H_2P are shifted and more extended with respect to the absorption counterparts. The differences have been attributed primarily to the change of the equilibrium geometry upon excitation, larger in H_2P and H_4P^{2+} than in $TOxP^{2+}$ and in the case of H_4P^{2+} to the nonplanar conformation of the macrocycle. Also the $S_1 \rightarrow S_0$ spectra of H_2P, H_4P^{2+}, and $TOxP^{2+}$ have been measured and more qualitatively discussed. The S_1 and S_2 fluorescence decays have been observed for H_4P^{2+} and $TOxP^{2+}$ exciting with ultrashort pulses. The S_2 lifetime of $TOxP^{2+}$ is of the order of the temporal resolution of our experimental apparatus, whereas that of H_4P^{2+} is shorter. The $S_2 \rightarrow S_0$ quantum yield of $TOxP^{2+}$ has been estimated to be 0.035, ∼3 orders of magnitude higher than that of H_4P^{2+}. It is proposed on the basis of ab initio model calculations that excited states of the $H_4P^{2+}(CF_3COO^-)_2$ complex with charge-transfer character are responsible of the increased extension of the $S_2 \rightarrow S_0$ spectrum with respect to that of H_2P.

I. Introduction

Porphyrins are fundamental protein components for a number of naturally occurring processes such as oxygen transport and storage in aerobic organisms, electron transfer in the intracellular respiratory chain, and electron and energy transfer in photosynthesis.[1] In the last years, several distorted porphyrins have been synthesized by substituent crowding at the periphery of the macrocycle[2,3] with the purpose of mimicking the modulation of reactivity in biological systems.[4,5] This has led us to study the correlation between conformational flexibility and photophysical properties in nonplanar porphyrinic prosthetic groups.[6,7] It was found that the S_1 ($\pi\pi^*$) lifetimes of distorted dodecaphenyl- and of tetra-*tert*-butylporphyrin at room temperature in nonpolar solvents are strongly reduced with respect to those of planar tetraphenyl- and octaethylporphyrin.[6,7] Correspondingly, a model was proposed where the nonplanar macrocycle, following the photoexcitation and the increase of conformational freedom into the S_1 state, shifts to funnel geometries where S_1 and S_0 are close in energy, thus enhancing the deactivation channel of internal conversion.[6,7]

Alternatively, diprotonated porphyrins may serve as simple yet attractive systems to investigate the influence of nonplanarity on the macrocycle photophysics. In this respect, work on substituted nonplanar porphyrin diacids has already appeared.[8−10] For instance, in diprotonated octaethylporphyrin (H_4OEP^{2+}) and tetraphenylporphyrin (H_4TPP^{2+}), the increase of the $S_1 \rightsquigarrow S_0$ nonradiative decay relative to the neutral species was observed.[8] It seems however that little attention has been devoted to the diprotonated species of unsubstituted porphyrin (H_4P^{2+}; **2** in Figure 1). Although no direct structural information is available, X-ray results on closely related systems[11] and recent MO/DF ab initio calculations[10,12,13] on H_4P^{2+} give the common indication that the lowest ground state conformation is nonplanar, i.e., saddle-shaped with D_{2d} symmetry. Due to the absence of peripheral substituents, **2** is recommended to study the effect of macrocycle bare nonplanarity. A previous study[14] has reported on the shortening of the S_1 lifetimes from the parent planar

* To whom correspondence should be addressed. E-mail: piero.salvi@unifi.it.

† Also at Laboratorio Europeo di Spettroscopie non Lineari (LENS), Universitá di Firenze, via N. Carrara 1, 50019 Sesto Fiorentino, Firenze, Italy and at INOA-CNR, Largo E. Fermi 6, 50125 Firenze, Italy.

10.1021/jp0686846 CCC: $37.00
Published on Web 03/08/2007

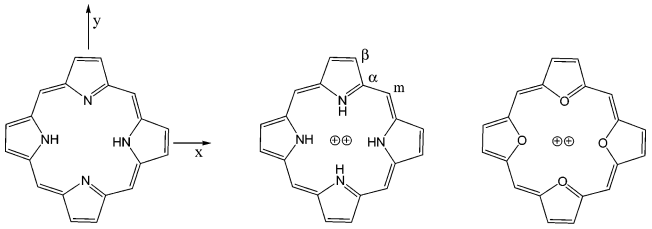

Figure 1. Molecular structures of porphyrin **1**, diprotonated porphyrin **2**, and tetraoxaporphyrin dication **3**. The reference system, common to the three species, is shown for convenience on **1**. The α, *β* and *meso* positions are indicated on **2**.

species (H_2P; **1** in Figure 1) to H_4P^{2+}, thus at least inviting an investigation about the possible dependence. Since in the course of a near-resonance Raman experiment on **2** a diffuse emission underlying the Raman peaks was observed[13] and tentatively assigned as fluorescence from the Soret band,[14] we felt motivated to undertake the study, performing fluorescence experiments on the S_2 state. As a major result of this work, it turns out that in addition to the conformational distortion other factors contribute to the shape of the $S_2 \rightarrow S_0$ spectrum, namely the shift of the S_2 equilibrium geometry with respect to the ground state and the occurrence of excited states of charge-transfer character[9,10] belonging to the complex $H_4P^{2+}(CF_3COO^-)_2$.

In order to discuss the relative weight of these factors in H_4P^{2+} it is convenient to make a comparison with suitable planar porphyrinic systems ("normal" according to a previous classification[6]). A straightforward choice might be H_2P on the basis of the overall photophysical behavior in the S_1 state, including the negligible shift between absorption and fluorescence origins and the S_1 lifetime[14] in the range of those of essentially planar substituted porphyrins.[6] However, this is arguable for states higher than S_1. It would be desirable to rely on a normal system with an energy diagram of the lowest $\pi\pi^*$ states paralleling as much as possible that of H_4P^{2+}. It luckily happened that tetraoxaporphyrin dication ($TOxP^{2+}$; **3** in Figure 1) fulfills the requirement and moreover shows strong fluorescence from both the S_1 and S_2 states. As a result, $TOxP^{2+}$ has been taken as reference for a discussion of the S_2 data on H_4P^{2+}. S_1 and S_2 lifetimes as well as $S_1 \rightarrow S_0$ and $S_2 \rightarrow S_0$ quantum yields have been measured which provide the first set of photophysical data on this interesting analogue of porphyrin.

II. Experimental Section

Porphyrin **1** has been purchased from Frontier Scientific (U.S.A.) and used without further purification. The perchlorate salt of tetraoxaporphyrin dication **3**, whose synthesis has been reported,[15] has been kindly provided by Prof. E. Vogel (University of Köln, Germany). The diprotonated species **2** is obtained in benzene solution by addition of a small amount (5% in volume) of trifluoroacetic acid which converts completely **1** to **2**.[14]

Solutions of **1**−**3** were freshly prepared using as solvents benzene for **1**, benzene and trifluoracetic acid for **2** and concentrated $HClO_4$ for **3**. The fluorescence spectra were taken with sample concentration in the range 10^{-4}−10^{-7} M. The absorption spectrum at the end of each fluorescence experiment was found to be substantially coincident with the absorption spectrum before experiment. No difference in the fluorescence profiles was noticed varying the concentration within the above-mentioned limits. Each solution spectrum was duplicated by that of the solvent alone, devoid of emission bands in the spectral region of interest. The fluorescence spectra were measured by means of a Perkin-Elmer spectrophotofluorimeter. The $S_1 \rightarrow S_0$ spectra of **1**−**3** were corrected above 600 nm due to the low efficiency of the emission monochromator in the red region of the visible. To this purpose, the fluorescence spectrum of Rhodamine 6G perchlorate ($c = 6 \times 10^{-4}$ M in ethanol) was compared with the reference spectrum,[16] and the correction factor was applied at each wavelength to the $S_1 \rightarrow S_0$ spectrum of the three species.

Fluorescence lifetimes were measured with ultrashort pulses (duration ≈ 300 fs at 1 kHz repetition rate, ≈1 μJ energy) from a regenerative Ti:sapphire laser system equipped with an optical parametric generator and amplifier (OPG-OPA). Nonlinear sum frequency and second harmonic generation in BBO crystals provide tunable laser pulses in the 240−800 nm spectral range thus achieving the proper excitation wavelength.[17] The fluorescence was collected through a quartz lens and focused onto a photocathode of a microchannel plate photomultiplier, after elimination of the incident scattered radiation by the appropriate set of colored filters. The photomultiplier signal was fed into a digital oscilloscope, 1.7 GHz band-pass, grounded through a 50 Ω resistor. The slightly asymmetric instrumental function, measured by light scattering from a latex solution, has a time duration (fwhh) of 550 ps, highly reproducible from one experiment to another. The experimental time profiles were deconvoluted taking into account the instrumental function and were at once fitted to exponentials. Then, intrinsic fluorescence lifetimes were obtained. Aerated and N_2-purged solutions of **1**−**3** were excited into the Soret and Q bands. Samples prepared in either way gave substantially equal time profiles, except for the $S_1 \rightarrow S_0$ fluorescence decay of **1**, with time constant 10.7 ns when the solution is aerated and 15.8 ns when deoxygenated ($\lambda_{exc} = 489$ nm), in good agreement with the reported value.[14] The $S_1 \rightarrow S_0$ profiles were found to be independent of the excitation wavelength, 489 and 390 nm for **1**, 544 and 370 nm for **2**, and 527 and 370 nm for **3**.

As to **3**, the $S_2 \rightarrow S_0$ quantum yield was measured comparing the fluorescence spectrum with that of a known standard and using dilute solutions in order to minimize reabsorption effects, as suggested.[18,19] With a 1 cm thick cell, the absorbance did not exceed 0.1 for the Soret maximum of **3** and for the $S_1 \rightarrow S_0$ of the reference molecule, 9-phenylanthracene (PA; $\eta_{S_1 \rightarrow S_0} = 0.49$, $\lambda_{exc} = 365$ nm, cyclohexane[16]). In turn, the standard has been cross-calibrated with 9,10-diphenylanthracene (DPA; $\eta_{S_1 \rightarrow S_0} = 1.0$, $\lambda_{exc} = 265$ nm, cyclohexane[16]). Keeping absorbances as low as stated above, the integrated fluorescence intensities of the two species are linearly proportional to absorbances. With the same excitation wavelength and solvent, quantum yields are found from the simple expression $(\eta_A/\eta_B) = (m_A/m_B)$ where A and B are the two components, DPA and PA, and m_A and m_B the slopes of the A and B linear plots. Cross-calibration gives 0.52 for PA and 0.95 for DPA with quantum yield ratio independent of λ_{exc} in the range 365−325 nm.

III. Results

A. Absorption and Fluorescence Spectra. The absorption and fluorescence spectra of diluted solutions ($c = 5 \times 10^{-6}$ M or less) of **1**−**3** at room temperature are shown in Figures 2−4. The excitation wavelengths of the fluorescence spectra shown in the Figures are 350 nm for **1** and **2** and 365 nm for **3**. The absorption spectra of the three molecules have been already reported[12,14,20−23] and discussed making reference to the well-known four-orbital model of porphyrins.[20,24] Here we add

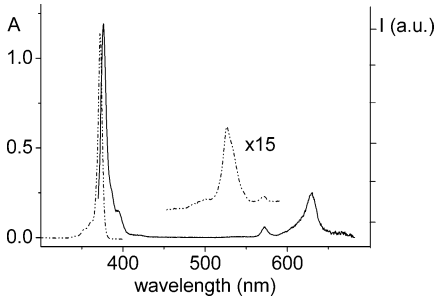

Figure 2. Absorption (long dash, double short dash; —--) and fluorescence (full line; $\lambda_{exc} = 365$ nm) spectra of **3**, $c = 10^{-6}$ M in concentrated $HClO_4$, at room temperature in the 300−700 nm spectral range. The absorbance scale (*A*) is on the left and the fluorescence scale (*I*, a.u.) on the right.

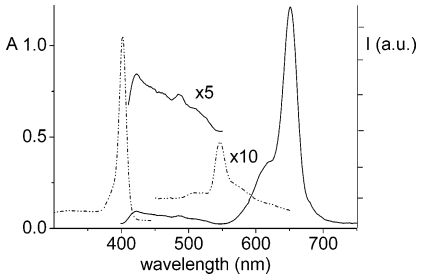

Figure 3. Absorption (long dash, double short dash; —--) and fluorescence (full line; $\lambda_{exc} = 350$ nm) spectra of **2**, $c = 4 \times 10^{-6}$ M in benzene solution added with CF_3COOH (5% in volume), at room temperature in the 300−700 nm spectral range. The absorbance scale (*A*) is on the left and the fluorescence scale (*I*, a.u.) on the right.

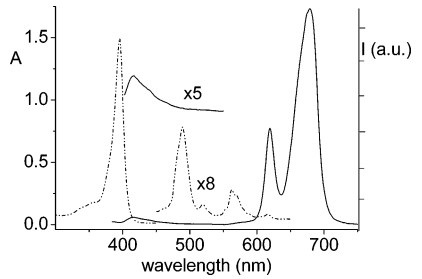

Figure 4. Absorption (long dash, double short dash; —--) and fluorescence (full line; $\lambda_{exc} = 350$ nm) spectra of **1**, $c = 5 \times 10^{-6}$ M in benzene solution, at room temperature in the 300−700 nm spectral range. The absorbance scale (*A*) is on the left and the fluorescence scale (*I*, a.u.) on the right.

TABLE 1: Summary of Spectral and Photophysical Data on the Lowest Excited States of 1−3: Absorption/Emission Shifts ΔE(abs/em) (cm^{-1}), Oscillator Strengths *f*, Fluorescence Quantum Yields η, Observed Fluorescence Lifetimes τ_f (ns), and Calculated Radiative Lifetimes τ_R (ns) from the Strickler−Berg Relation (See Ref 27)

		ΔE(abs/em)	*f*	η	τ_f	τ_R
1	Q_x	65	0.02[a]	0.054[b]	15.8	238.
	Q_y		0.07[a]			
	B_x;B_y	1210	1.15[a]			1.9
2	Q		0.045	0.046[b]	5.5	133.
	B	1205	1.17	5.6×10^{-5}[b]	1.5×10^{-4}[c]	2.6
3	Q	15	0.046	0.11	7.3	100
	B	285	2.0	0.035	≤ 0.1;0.04[c]	1.1

[a] From ref 22. [b] From ref 14. [c] Estimated from quantum yield measurements.

information pertinent to the comparison with the fluorescence spectra, starting for the sake of convenience from **3**. Table 1 summarizes spectral and photophysical data collected on **1**−**3** in this and past[14,22] studies.

1. TOxP^{2+}. Under D_{4h} symmetry,[13,15,25] the two lowest excited states of **3** may be described as minus and plus combinations of excited configurations resulting from the promotion of one electron from the highest occupied MO's, a_{2u} and a_{1u}, to the doubly degenerate e_g LUMO orbital.[23] The $S_0 \rightarrow S_1$ and $S_0 \rightarrow S_2$ transitions are allowed being S_1 and S_2 of E_u symmetry and give origin to the so-called Q and B (or Soret) bands, respectively. The first transition is weakly allowed and the second strongly allowed because of the near equality of the transition moments from the ground to the two excited configurations. The observed absorption spectrum (see Figure 2) agrees well with these predictions. The Q-band is by far less intense than the B band. The electronic origin of the Q-band is observed as a very weak peak at 17 495 cm^{-1} (571.5 nm), whereas that of the B band shows prominently at 26 865 cm^{-1} (372.2 nm) as a sharp peak with a remarkably low bandwidth, Γ (fwhm) ≈ 415 cm^{-1}. The intense vibronic band 1515 cm^{-1} above the Q origin borrows intensity much probably through S_1/S_2 coupling. On the contrary, the Soret origin dominates largely over the ensuing vibronic structure with intervals 865 and 1445 cm^{-1}.

Going now to the fluorescence results, two strong emissions are observed in the range 375−400 nm and 570−670 nm with a marked mirror symmetry with respect to the absorption profile. This is a clear indication of assignment as B and Q fluorescence, respectively. The onset of the Q fluorescence occurs at 17480 cm^{-1} (572.0 nm), 15 cm^{-1} to the red of the absorption origin. This shift is even smaller than those reported for "normal" peripherally substituted porphyrins.[6] The B fluorescence has an origin at 26 580 cm^{-1} (376.2 nm) with a red shift from the absorption origin of 285 cm^{-1}. Neither $S_2 \rightarrow S_0$ nor $S_1 \rightarrow S_0$ fluorescence profiles change as the excitation is varied up to 300 nm.

2. H$_4$*P*$^{2+}$. Under D_{2d} symmetry[13,12] the absorption pattern of **2** is expected to be similar to that of **3** (i.e., still consisting of Q and B bands with highly different intensities), assigned as $A_1 \rightarrow E$ transitions due to symmetry lowering (see Figure 3). On the whole, spectral broadening increases going from **3** to **2**. The Soret band is found at 24 875 cm^{-1} (402.0 nm) with width Γ (fwhm) ≈ 810 cm^{-1}. In the Q-band system, a single peak is observed at 18 310 cm^{-1} (546.2 nm) and a long unstructured tail extending beyond ≈16 600 cm^{-1} (≈ 600 nm).

Our fluorescence spectra, relative to the $S_1 \rightarrow S_0$ and $S_2 \rightarrow S_0$ emissions, are in good agreement with reported data.[14] In the $S_1 \rightarrow S_0$ spectrum, a single strong band is seen at 15 360 cm^{-1} (≈ 651.0 nm), assigned as fluorescence counterpart of the 18 310 cm^{-1} absorption band. The energy difference, 2950 cm^{-1}, depends on the vibrational frequency of the excited mode in S_0 and S_1 and on the gap between the absorption and fluorescence origins. Thus, on this basis, no accurate estimate of the absorption/fluorescence shift can be given. This parameter however should be small since for H_4OEP^{2+}, exhibiting a spectral pattern similar to H_4P^{2+} both in absorption and in fluorescence,[8] the shift is modest, ≈ 130 cm^{-1}. On the contrary, the $S_2 \rightarrow S_0$ band maximum is observed at 23 670 cm^{-1} (422.5 nm), 1205 cm^{-1} to the red of the absorption band. The spectrum extends down to 18 200 cm^{-1} (≈ 550 nm), in contrast with the relatively narrow range of the $S_0 \rightarrow S_2$ absorption.

3. H$_2$*P*. The absorption spectrum of **1** in benzene solution is known.[22] Lowering the molecular symmetry from D_{4h} in **3** to D_{2h} in **1**, the two lowest excited states of E_u symmetry species split each into two components, one B_{3u} and one B_{2u}. Accordingly, the Q and B absorptions give origin to four bands, Q_x (B_{3u}) and Q_y (B_{2u}) and B_x (B_{3u}) and B_y (B_{2u}). Our spectrum is

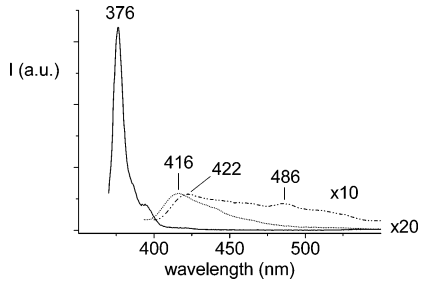

Figure 5. $S_2 \rightarrow S_0$ fluorescence spectra of **1** (short dash; ---), **2** (long dash, double short dash, —--), and **3** (full line), in the same experimental conditions described in Figures 2−4.

reported in Figure 4. Experimentally, Q_x and Q_y are well separated with origins at 16 205 cm^{-1} (617.0 nm) and at 19 230 cm^{-1} (520.0 nm). The Q_x transition shows also two vibronic additions at 17 590 and 17 720 cm^{-1}, 1385 and 1515 cm^{-1} from the origin, while the Q_y transition only one at 20 490 cm^{-1} (≈ 488 nm), assigned as 19 230 + 1260 cm^{-1}. The Soret band due to unresolved B_x and B_y transitions is observed with maximum at 25 250 cm^{-1} (396 nm) and width Γ (fwhm) ≈ 1070 cm^{-1}.

The intense and well-structured $Q_x \rightarrow S_0$ emission has origin at 16 150 cm^{-1} (619.2 nm), 55 cm^{-1} to the red of the absorption origin. An intense vibronic band is observed at 14 730 cm^{-1} (≈ 679.0 nm), 1420 cm^{-1} lower than the fluorescence origin. The Soret fluorescence of free-base porphyrins has been rarely observed.[26] According to our results, the unstructured spectrum extends down to ≈ 20 000 cm^{-1} (500 nm) with maximum at 24 040 cm^{-1} (≈ 416 nm, see Figure 4). The absorption/emission shift results 1210 cm^{-1}. The $S_2 \rightarrow S_0$ fluorescence spectra of the three species, **1**−**3**, have been collected in Figure 5.

B. Fluorescence Lifetimes and Quantum Yields. *1. TOxP²⁺*. The time profiles of the B and Q fluorescences have been measured at room-temperature exciting the sample ($c = 2 \times 10^{-7}$ M in concentrated $HClO_4$) with 527 and 370 nm pulses. As it is seen in Figure 6, the Q fluorescence decay is monoexponential, $\tau_{S_1 \rightarrow S_0} = 7.3$ ns, deconvolving the temporal line shape from the instrumental function. Exciting with 370 nm pulses the S_1 lifetime is substantially the same, 7.2 ns.

The B fluorescence evolves in a time interval comparable to that of the instrumental function (see Figure 6). The lifetime is shorter than 550 ps but cannot be determined with accuracy applying the deconvolution procedure. Reasonably, an upper limit of ≈100 ps may be set to the S_2 lifetime. On the other hand, $\tau_{S_2 \rightarrow S_0}$ may be calculated knowing the radiative (R) lifetime and the fluorescence quantum yield. To this purpose $\eta_{S_2 \rightarrow S_0}$ has been evaluated from the plot of the integrated fluorescence intensities vs absorbances, according to the procedure outlined in the Experimental Section, and comparing with the linear PA plot. With $n_{HClO_4} = 1.416$ and $n_{C_6H_{12}} = 1.426$ and for the excitation in the spectral range 365−325 nm, $\eta_{S_2 \rightarrow S_0}$ is constant, equal to 0.035, using the expression $(\eta_A/\eta_B) = (m_A/m_B)(n_A/n_B)^2$ where A is $TOxP^{2+}$ and B is PA. From the Strickler and Berg relation[27] the S_2 radiative lifetime is calculated ≈1.1 ns so that $\tau_{S_2 \rightarrow S_0} = \eta_{S_2 \rightarrow S_0} \tau_{R,S_2 \rightarrow S_0} \approx 40$ ps. For the sake of completeness quantum yield measurements have been extended to S_1. It was found $\eta_{S_1 \rightarrow S_0} = 0.11$ by comparison with the quantum yield of Rhodamine 6G ($\eta_{S_1 \rightarrow S_0} = 0.98$, $\lambda_{exc} = 514$ nm, methanol[28]).

The surprisingly high $S_2 \rightarrow S_0$ fluorescence yield is worth of further comment. $S_2 \rightarrow S_0$ fluorescence is observed in some metalloporphyrins.[14,29−32] For instance, in Zn, Al, Ga, and In porphyrins,[14] $S_2 \rightarrow S_0$ fluorescence was observed with a yield

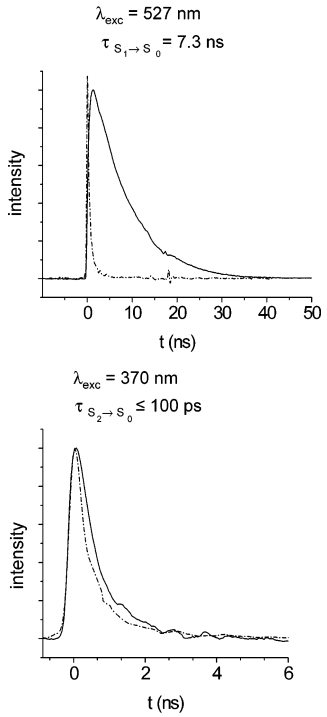

Figure 6. Observed decay profiles (full lines) for the $S_1 \rightarrow S_0$ (top) and $S_2 \rightarrow S_0$ (bottom) fluorescence of $TOxP^{2+}$ exciting with pulses at 527 and 370 nm, respectively. The time constants for the $S_2 \rightarrow S_0$ and $S_1 \rightarrow S_0$ fluorescence are indicated. The instrumental function (dash-dot) is also shown in the figure. A finite difference between the instrumental function and the $S_2 \rightarrow S_0$ fluorescence decay is observed.

in the 10^{-4}−10^{-5} range, approximately 2−3 orders of magnitude less than $\eta_{S_2 \rightarrow S_0}$ ($TOxP^{2+}$). Upon S_2 excitation, fast relaxation processes occur in metalloporphyrins due to the charge transfer from the porphyrin macrocycle to the central transition metal and to the back-donation from the metal to porphyrin.[33] This makes plausible the large difference between $\eta_{S_2 \rightarrow S_0}$ ($TOxP^{2+}$) on one side and $\eta_{S_2 \rightarrow S_0}$ of metalloporphyrins on the other. $S_n \rightarrow S_0$ ($n \geq 2$) fluorescence has also been reported for other, mostly aromatic, molecules.[34−37] In the classic example of azulene, the $S_2 \rightarrow S_0$ fluorescence was related to the anomalously large S_2−S_1 energy gap.[34] In the case of $TOxP^{2+}$, the occurrence of a sharp Soret band with a very high extinction coefficient[15] ($\epsilon_{372} = 10^6$ M^{-1} cm^{-1}) far from the Q-band (ΔE(B-Q) = 9370 cm^{-1}) and the presumable absence of intermediate states between B and Q give the unusual result of the yield from the B state comparable to that from the Q state. As to azulene, the correlation fluorescence yield−energy gap was verified tuning the gap with azulene derivatives or by using different solvents and observing the corresponding change of the nonradiative decay rate.[38] As to $TOxP^{2+}$, unfortunately, experimental conditions such as insolubility in common organic solvents and decomposition in water[15] made other preparations not feasible.

2. H_4P^{2+}. The fluorescence time profiles of H_4P^{2+} ($c \approx 10^{-6}$ M in benzene/CF_3COOH 5% v/v) are displayed in Figure 7. Within the experimental error, the S_1 lifetime of 5.5 ns is independent of the excitation wavelength, 544 and 370 nm, and of the purging process. Combining the S_1 lifetime with quantum yield,[14] $\eta_{S_1 \rightarrow S_0} = 0.046$, the radiative lifetime $\tau_{R,S_1 \rightarrow S_0}$ is calculated to be ≈120 ns, which compares satisfactorily with the value of 133 ns derived from the Strickler and Berg relation.[27] On the contrary, the observed decay of the B fluorescence fully overlaps the instrumental line shape (see Figure 7) and cannot be used for a lifetime determination. A rough estimate of $\tau_{S_2 \rightarrow S_0}$ is attempted considering the quantum

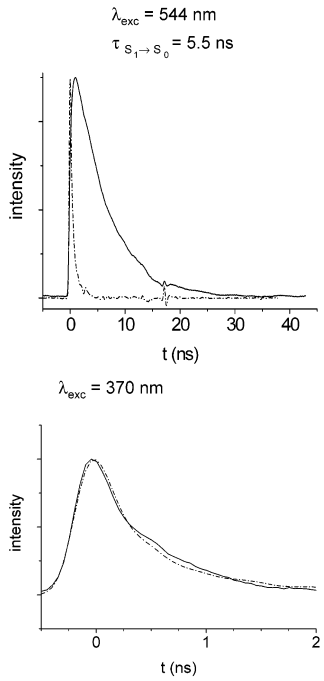

Figure 7. Observed decay profiles (full lines) for the $S_1 \rightarrow S_0$ (top) and $S_2 \rightarrow S_0$ (bottom) fluorescence of H_4P^{2+} exciting with pulses at 544 and 370 nm, respectively. The time constant for the $S_1 \rightarrow S_0$ fluorescence is indicated. As to $S_2 \rightarrow S_0$, the decay process occurs in a time below the temporal resolution of the experimental apparatus. The instrumental function (dash-dot) is also shown in the figure.

yield for the $S_2 \rightarrow S_0$ fluorescence,[14] 5.6×10^{-5}, and the radiative S_2 lifetime, calculated to be ≈2.6 ns. This gives a value of ≈150 fs for $\tau_{S_2 \rightarrow S_0}$.

IV. Discussion

$TOxP^{2+}$ may be classified as a normal[6] porphyrin analogue on the basis of S_1 and S_2 data. Considering the S_1 state, the most significant properties are the small shift, 15 cm^{-1}, between absorption and fluorescence origins, the vibronic structure of both spectra, the S_1 lifetime in the range of those of planar substituted porphyrins[6] and of H_2P.[14] As to S_2, it should be mentioned the moderate absorption/emission shift, the clear mirror symmetry between sharp absorption and fluorescence bands and the independence of fluorescence on the excitation wavelength. These are good indications that the square D_{4h} symmetry of the ground state structure[13,15,25] is conserved in S_1 and S_2 and that the equilibrium geometries in these states do not differ appreciably from that of S_0; that is, the minima are only weakly displaced each with respect to the other. Comparing with $TOxP^{2+}$, both H_2P and H_4P^{2+} exhibit (1) increased but approximately equal shifts between S_2-S_0 absorption and fluorescence maxima (see Table 1); (2) extended and structureless $S_2 \rightarrow S_0$ fluorescence spectra (see Figure 5), and (3) as to H_4P^{2+}, a shorter estimated S_2 lifetime (see Table 1).

Going first to discuss the S_2 absorption/fluorescence shifts, we recall that near-resonant Raman experiments on H_4P^{2+} exciting at 406.7 nm have characterized the S_2 equilibrium geometry as more expanded and less distorted with respect to that of the ground state.[13] In fact, the Raman lines at 310, 1384, and 238 cm^{-1}, which show the largest intensity enhancement at this excitation wavelength, were assigned to totally symmetric modes, the first two as combinations of $C_\alpha N$ and $C_\alpha C_\beta$ stretchings with the $C_\alpha C_m C_\beta$ bending and the third as due to pyrrole torsions.[13] The three vibrational modes favor the delocalization of π electrons along the ring and, in particular the third, 238 cm^{-1} partially relieves the macrocycle nonplanarity. Since the 310 and 1384 cm^{-1} a_1 modes of H_4P^{2+} correlate with the 312 and 1352 cm^{-1} a_g modes of H_2P and the latter are the most intense a_g peaks of the H_2P Raman spectrum in the same excitation conditions,[13] it is concluded that also the H_2P macrocycle has in S_2 a planar equilibrium geometry more expanded than in S_0. The change of the equilibrium geometry upon excitation is responsible of the S_2 shift comparably in H_4P^{2+} and in H_2P.

TABLE 2: Observed[a] Core Conformations of H_4OEP^{2+} and H_4TPP^{2+} and Calculated (DF/B3-LYP/cc-pVDZ) Core Conformations of 2 in D_{2d} and C_i Symmetry[b]

	2;C_i	$(H_4OEP)^{2+}$	**2**;D_{2d}	$(H_4TPP)^{2+}$
$\|C_\alpha\|$	0.14	0.12	0.16	0.28
$\|C_\beta\|$	0.08	0.48	0.49	0.93
$\|C_m\|$	0.17	0.28	0.	0.02
$\|C_{20}\|$	0.12	0.30	0.26	0.48
$\|N_4\|$	0.21	0.31	0.02	0.08
$\|C_{20}N_4\|$	0.14	0.30	0.22	0.42

[a] From ref 11. [b] As defined in ref 11, $|C_\alpha|$, $|C_\beta|$, $|C_m|$, $|C_{20}|$, $|N_4|$, and $|C_{20}N_4|$ are the mean absolute perpendicular displacements (Å) of the α-, β-, meso-, 20-porphyrin carbons, pyrrole nitrogens and 24 core atoms from the 24 atoms mean plane of the porphyrin.

In substituted porphyrin diacids $S_1 \rightarrow S_0$ broadening has been related to the larger flexibility with respect to the planar species and to a higher number of nearly isoenergetic structures accessible in the ground/excited states.[8] Experimental data have been reported[8] showing that the conformational factor does not affect to the same extent the spectral properties of H_4OEP^{2+} and H_4TPP^{2+} and indicate that H_4OEP^{2+} is less flexible than H_4TPP^{2+}. The similarity of vibronic structure in the $S_0 \rightarrow S_1$ and $S_1 \rightarrow S_0$ spectra of H_4P^{2+} and H_4OEP^{2+} suggests the same conclusion for H_4P^{2+}. The result may be rationalized noting that for diprotonated species a measure of their deviation from planarity is the set of average absolute perpendicular displacements of the ring C atoms (α, β, meso C atoms, see Table 2 for more detail) from the 24-atom porphyrin mean plane.[11] In the absence of X-ray data on H_4P^{2+}, we make reference to recent MO/DF structural results.[10,12,13] H_4P^{2+} is known to adopt two stable (i.e., corresponding to all real vibrational frequencies) conformational structures in the ground state, one saddle (D_{2d}; lower) and one quasiwave (C_i; upper), separated by 5.1−5.3 kcal/mol, respectively[10,12,13] (see Figure 8). The calculated set of values for the two minima, **2**;D_{2d} and **2**;C_i, are compared in Table 2 with those experimentally observed[11] for the two distorted diacids, H_4OEP^{2+} and H_4TPP^{2+}. From the dispersion of the absolute displacements it may be seen that the macrocycle distortion increases in the order **2**;C_i < H_4OEP^{2+} < ≈**2**;D_{2d} < H_4TPP^{2+}, in good agreement with the previous conclusion.

The $S_2 \rightarrow S_0$ spectrum of H_4P^{2+} is more diffuse than that of $TOxP^{2+}$ (see Figure 5). A combination of factors may be envisioned for this change. Consider first the conformational flexibility taking into account the vibrational frequencies on isolated $TOxP^{2+}$ and H_4P^{2+} systems.[13] Distortion modes of a planar macrocycle such as $TOxP^{2+}$ may be classified[39−41] as ruffling, saddling, doming, and waving modes and belong to the b_{1u}, b_{2u}, a_{2u}, and e_g symmetry species, respectively, of the D_{4h} group. These are the normal modes of lowest frequency in each of the above-mentioned symmetry species[13] [i.e., 58 cm^{-1} (b_{1u}), 45 cm^{-1} (b_{2u}), 100 cm^{-1} (a_{2u}), 121 cm^{-1} (e_g)]. None of these modes is involved in an allowed vibronic transition of the fluorescence spectrum. Going from D_{4h} to D_{2d}, the correlation table is[13] $b_{1u} \rightarrow a_2$; $b_{2u} \rightarrow a_1$; $a_{2u} \rightarrow b_2$; $e_g \rightarrow e$; due to the loss of the inversion symmetry. The distortion modes conserve their character with frequencies shifted as in the following:[13]

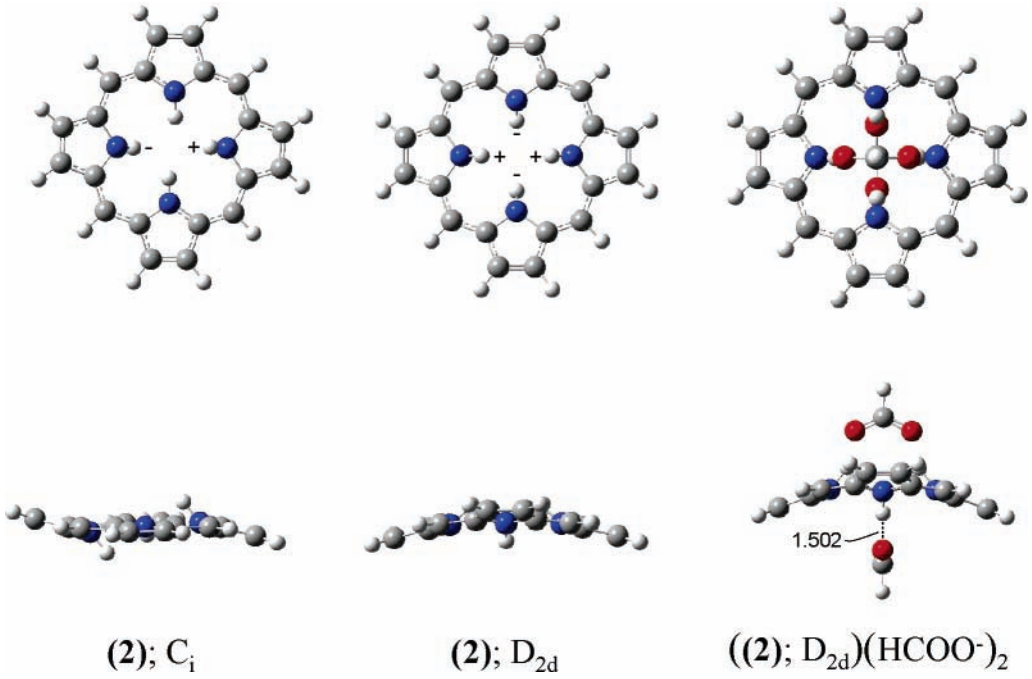

Figure 8. Top and side view of the two stable isomers of **2**, left C_i and center D_{2d}, and of the (**2**;D_{2d})$(HCOO^-)_2$ complex, according to our DF/B3-LYP/cc-pVDZ calculation. Plus and minus signs indicate qualitatively the arrangement of the pyrrole ring above (+) and below (−) the mean porphyrin plane.

58 cm^{-1} (b_{1u}) → 69 cm^{-1} (a_2); 45 cm^{-1} (b_{2u}) → 59 cm^{-1} (a_1); 100 cm^{-1} (a_{2u}) → 85 cm^{-1} (b_2), 121 cm^{-1} (e_g) → 127 cm^{-1} (e). Due to symmetry lowering, the origin and vibronic S_2-S_0 transitions may be combined with the fundamental level of the 59 cm^{-1} (a_1) mode giving additional allowed transitions. Upon normal mode inspection,[13] it is seen that the 59 cm^{-1} torsion is related to molecular flexibility, inducing the saddle-shaped D_{2d} structure to be more planar and favoring the change of the equilibrium geometry from the ground to the excited state.

From Figure 5, it may be observed that the emission of **2** is extended over a range wider than for **1**. Subtraction between the two spectra gives a band roughly centered around 486 nm. Two assignments have been hypothesized for this feature, i.e., fluorescence either from the second conformer of **2**, S_2 (**2**;C_i) → S_0 (**2**;C_i), or from the lowest charge transfer state of the complex (**2**;D_{2d})$(CF_3COO^-)_2$, following a recent suggestion.[9,10] A reasonable indication is given on the basis of MO calculation. By means of the Gaussian program,[42] we have performed TD−DFT calculations of vertical excitation energies for **2**;D_{2d} and **2**;C_i with the B3-LYP functional and the cc-pVDZ basis set and promoting electrons from the higher 40 occupied MOs to the lower 120 virtual MOs in a singly excited configuration interaction scheme. Our results on **2**;D_{2d} compare well with recent calculations,[12] predicting a first vertical transition, S_0 (A_1) → S_1 (E), at 2.33 eV (≈532 nm) and a second, S_0 (A_1) → S_2 (E), at 3.63 eV (≈341 nm). Under C_i symmetry each transition splits into a doublet (both components of A_u species) at 2.32;2.37 eV and at 3.63;3.70 eV. These energy values are not appreciably different from those of the D_{2d} conformer. A third, almost planar, conformer of C_s symmetry lies on a shallow maximum of the ground state surface (with a single imaginary frequency, 122*i* cm^{-1}) and has energy 5.6 kcal/mol higher than **2**;D_{2d}.[13] The calculation has been repeated for this maximum, and the values are 2.35 (A′); 2.36 (A ″) eV and 3.63 (A); 3.71 (A″) eV. Thus, excitation energies of H_4P^{2+} are not sensitive to the conformational structure, excluding the first hypothesis. The results are shown in Figure 9, where S_1 and S_2 indicate the two excited states under consideration. As to the second assignment, the

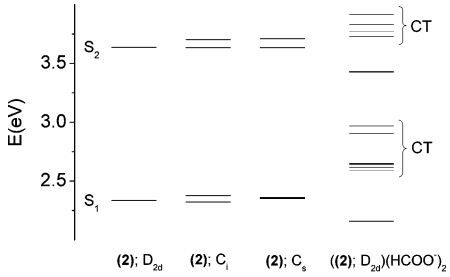

Figure 9. Vertical excitation energies (eV, TD−DFT/B3-LYP/cc-pVDZ results) from the ground to the lowest excited states of diprotonated porphyrin. **2**;D_{2d} and **2**;C_i: conformational minima; **2**;C_s: shallow conformational maximum; (**2**;D_{2d})$(HCOO^-)_2$: complex with two formiate ions. Energy levels of charge transfer state (i.e., with excitation from formiate ion to the macrocycle) are denoted as CT. Unmarked levels are associated with excited states mostly localized on the porphyrin macrocyle.

calculation has been carried out on a simplified complex, substituting the trifluoroacetate with the formiate counterion in order to preserve the D_{2d} symmetry. The optimized geometry of the complex (**2**;D_{2d})$(HCOO^-)_2$ reported in Figure 8 has the counterion in close contact with the macrocycle, the four O•• •H distances being as short as 1.502 Å. Two types of excited states are found. The first includes states arising from singly excited configurations built on MOs mostly localized on the macrocycle ring. These are $\pi\pi^*$ states approximately similar to the S_1 and S_2 states of the isolated H_4P^{2+}. Due to the counterion, vertical transitions from the ground to these states, of *E* symmetry, shift to lower energies, 2.16 eV (≈574 nm) and 3.42 eV (≈362 nm), in close agreement with the experimental absorption spectrum of **2**. The second set of states are described as due to electron promotion from occupied MOs localized on the formiate counterion to virtual MOs localized on the porphyrin macrocycle. These are charge transfer (CT) states. From our calculations, they are interspersed between S_1 and S_2 or at an energy higher than S_2, as it may be seen from Figure 9. The lowest CT states, having vertical excitation energies 2.59 eV (≈478 nm) and 2.62 eV (≈473 nm) and

oscillator strengths ≈0.01, more than twice that associated with S_1 ($\pi\pi^*$), belong to *E* symmetry and are active in a fluorescence transition. If the lowest CT states are weakly coupled with S_1-($\pi\pi^*$), the second assignment is plausible. The occurrence of CT states between S_1 and S_2 also justifies, on the basis of the internal $S_2 \rightsquigarrow$ CT conversion, the decrease of the S_2 lifetime in H_4P^{2+} $(CF_3COO^-)_2$ with respect to $TOxP^{2+}$ down to the picosecond/subpicosecond time regime.

V. Conclusions

The emission properties of nonplanar diprotonated porphyrin, planar porphyrin, and tetraoxaporphyrin dication upon photoexcitation in the S_2 state have been investigated at room temperature in solution. All of these molecular species fluoresce not only from S_1 but also from S_2. The $S_2 \rightarrow S_0$ spectrum of $TOxP^{2+}$ has been easily observed due to peculiarities of the system, i.e., a high $S_0 \rightarrow S_2$ oscillator strength, a large S_2-S_1 energy gap, and an absence of states within the gap. Fluorescence quantum yields and lifetimes have been determined. On the contrary, the Soret fluorescence spectra of H_2P and H_4P^{2+} are perturbed with respect to $TOxP^{2+}$ (i.e., considerably redshifted from the absorption band and more extended). These spectral differences have been discussed in terms of molecular flexibility, due to low-frequency vibrational modes, and change of equilibrium geometry between S_0 and S_2. As to H_4P^{2+} only, it has been proposed that the fluorescence emission is also related to charge-transfer states of the complex $H_4P^{2+}(CF_3COO^-)_2$. Overall, the photophysical parameters of diprotonated porphyrin in the S_2 state are correlated not to a single but rather to a set of molecular properties. Time-resolved measurements on the S_1 state have shown that the S_1 lifetimes of H_4P^{2+} and $TOxP^{2+}$ are in the range of those of planar porphyrins. Exciting into the S_2 state both molecular species relax within (or comparably to) the time resolution of the experimental apparatus. Indirect estimates of S_2 lifetimes from quantum yield measurements and radiative lifetimes wait corroboration from direct transient absorption experiments actually under way in our laboratory.

Acknowledgment. The authors are grateful to Prof. E. Vogel (University of Köln, Germany) for the generous gift of a sample of tetraoxaporphyrin perchlorate and to Dr. Gabriella Caminati (Department of Chemistry, University of Florence) for the use of the Perkin−Elmer spectrofluorimeter. This work was supported by INSTM under the Contract FIRB RBNE033KMA and by the European Community under the Contract RIII−CT-2003-506350.

References and Notes

(1) *The Porphyrins, vol. I - VII*; Dolphin, D., Ed.; Academic Press: New York, 1978.
(2) Medforth, C. J.; Senge, M. O.; Smith, K. M.; Sparks, L. D.; Shelnutt, J. A. *J. Am. Chem. Soc.* **1992**, *114*, 9859−9869.
(3) Medforth, C. J.; Berber, M. D.; Smith, K. M. *Tetrahedron Lett.* **1990**, *31*, 3719−3722.
(4) Crane, B. R.; Siegel, L. M.; Getzoff, E. D. *Science* **1995**, *270*, 59−67.
(5) Shelnutt, J. A.; Song, X. Z.; Ma, J.-G.; Jia, S.-L.; Jentzen, W.; Medforth, C. J. *Chem. Soc. Rev.* **1998**, *27*, 31−41.
(6) Gentemann, S.; Medforth, C. J.; Forsyth, T. P.; Nurco, D. J.; Smith, K. M.; Fajer, J.; Holten, D. *J. Am. Chem. Soc.* **1994**, *116*, 7363−7368.
(7) Gentemann, S.; Nelson, N. Y.; Jaquinod, L.; Nurco, D. J.; Leung, S. H.; Medforth, C. J.; Smith, K. M.; Fajer, J.; Holten, D. *J. Phys. Chem. B* **1997**, *101*, 1247−1254.
(8) Chirvony, V. S.; van Hoek, A.; Galievski, V. A.; Sazanovich, I. V.; Schaafsma, T. J.; Holten, D. *J. Phys. Chem. B* **2000**, *104*, 9909−9917.
(9) Knyukshto, V. N.; Solovyov, K.; Egorova, G. D. *Biospectroscopy* **1998**, *4*, 121−133.
(10) Avilov, I. V.; Panarin, A. Y.; Chirvony, V. S. *Chem. Phys. Lett.* **2004**, *389*, 352−358.
(11) Cheng, B.; Munro, O. Q.; Marques, H. M.; Scheidt, W. R. *J. Am. Chem. Soc.* **1997**, *119*, 10732−10742.
(12) Chen, D.-M.; Liu, X.; He, T.-J.; Liu, F.-C. *Chem. Phys.* **2003**, *289*, 397−407.
(13) Jelovica, I.; Moroni, L.; Gellini, C.; Salvi, P. R.; Orlic, N. *J. Phys. Chem. A* **2005**, *109*, 9935−9944.
(14) Ohno, O.; Kaizu, Y.; Kobayashi, H. *J. Chem. Phys.* **1985**, *82*, 1779−1787.
(15) Vogel, E.; Haas, W.; Knipp, B.; Lex, J.; Schmickler, H. *Angew. Chem., Int. Ed. Engl.* **1988**, *27*, 406−409.
(16) Berlman, I. *Handbook of Fluorescence Spectra of Aromatic Molecules*; Academic Press: New York, 1971.
(17) Neuwhal, F. V. R.; Bussotti, L.; Foggi, P. In *Res. Adv. Photochem. Photobiol*. Global Research Network: Trivandrum, India, 2000; Vol. 1, pp 77−94.
(18) Williams, A. T. R.; Winfield, S. A.; Miller, J. N. *Analyst.* **1983**, *108*, 1067−1071.
(19) Dhami, S.; DeMello, A. J.; Rumbles, G.; Bishop, S. M.; Plillips, D.; Beeby, A. *Photochem. Photobiol.* **1995**, *61*, 341−346.
(20) Gouterman, M. In *The Porphyrins*; Dolphin, D., Ed.; Academic Press: New York, 1978; vol. III, pp 1−165.
(21) Edwards, L.; Dolphin, D. H.; Gouterman, M.; Adler, A. D. *J. Mol. Spectrosc.* **1986**, *38*, 16−32.
(22) Nagashima, U.; Takada, T.; Ohno, K. *J. Chem. Phys.* **1986**, *85*, 4524−4529.
(23) Bachmann, A.; Gerson, F.; Gescheidt, G.; Vogel, E. *J. Am. Chem. Soc.* **1992**, *114*, 10855−10860.
(24) Gouterman, M. *J. Chem. Phys.* **1959**, *30*, 1139−1161.
(25) Malsh, K.; Roeb, M.; Karuth, V.; Hohlneicher, G. *Chem. Phys.* **1998**, *227*, 331−348.
(26) Akimoto, S.; Yamazaki, T.; I, Y.; Osuka, A. *Chem. Phys. Lett.* **1999**, *309*, 177−182.
(27) Strickler, S. J.; Berg, R. A. *J. Chem. Phys.* **1962**, *37*, 814−822.
(28) Lee, W. K.; Gungor, A.; Ho, P.; Davis, C. C. *Appl. Phys. Lett.* **1985**, *47*, 916−918.
(29) Bajema, L.; Gouterman, M.; Rose, C. B. *J. Mol. Spectry* **1971**, *39*, 421−431.
(30) Martarano, L. R.; Wong, C.-P.; W. D. Horrocks, J. Goncalves, A. M. P. *J. Phys. Chem.* **1976**, *80*, 2389−2393.
(31) Kurabayashi, Y.; Kikuchi, K.; Kokubun, H.; Kaizu, Y.; Kobayashi, H. *J. Phys. Chem.* **1984**, *88*, 1308−1310.
(32) Tsvirko, M. P.; Stelmakh, G. F.; Pyatosin, V. E.; Solovyov, K. N.; Kachura, T. F.; Piskarkas, A. S.; Gadonas, R. A. *Chem. Phys.* **1986**, *106*, 467−476.
(33) Sorges, S.; Poisson, L.; Raffael, K.; Krim, L.; Soep, B.; Shafizadeh, N. *J. Chem. Phys.* **2006**, *124*, 114302.
(34) Beer, M.; Longuet-Higgins, H. *J. Chem. Phys.* **1955**, *23*, 1390−1391.
(35) Horner, G.; Topp, M. *Chem. Phys. Lett.* **1975**, *36*, 295−300.
(36) Klann, R.; Bauerle, R.; Laermer, F.; Elsaesser, T.; Niemeyer, M.; Luttke, W. *Chem. Phys. Lett.* **1990**, *169*, 172−178.
(37) Gellini, C.; Salvi, P. R.; Hafner, K. *J. Phys. Chem.* **1993**, *97*, 8152−8157.
(38) Wagner, B.; Tittelbach-Helmrich, D.; Steer, R. *J. Phys. Chem.* **1992**, *96*, 7904−7908.
(39) Ravikanth, M.; Chandrashekar, T. K. *Struct. Bond.* **1995**, *82*, 105−188.
(40) Jentzen, W.; Simpson, M. C.; Hobbs, J. D.; Song, X.; Ema, T.; Nelson, N. Y.; Medforth, C. J.; Smith, K. M.; Veyrat, M.; Mazzanti, M.; Ramasseul, R.; Marchon, J.-C.; Takeuchi, T.; Goddard, W. A., III; Shelnutt, J. A. *J. Am. Chem. Soc.* **1995**, *117*, 11085−11097.
(41) Nurco, D. J.; Medforth, C. J.; Forsyth, T. P.; Olmstead, M. M.; Smith, K. M. *J. Am. Chem. Soc.* **1996**, *118*, 10918−10919.
(42) Frisch, M. J.; Trucks, G. W.; Schlegel, H. B.; Scuseria, G. E.; Gill, P. M. W.; Stratmann, R. E.; Burant, J. C.; Dapprich, S.; Millam, J. M.; Daniels, A. D.; Kudin, K. N.; Strain, M. C.; Farkas, O.; Tomasi, J.; Barone, V.; Cossi, M.; Cammi, R.; Mennucci, B.; Pomelli, C.; Adamo, C.; Clifford, S.; Ochterski, J.; Johnson, B. G.; Robb, M. A.; Cheeseman, J. R.; Keith, T.; Petersson, G. A.; Montgomery, J. A.; Raghavachari, K.; Al-Laham, M. A.; Zakrzewski, V. G.; Ortiz, J. V.; Foresman, J. B.; Cioslowski, J.; Stefanov, B. B.; Liu, G.; Liashenko, A.; Piskorz, P.; Komaromi, I.; Cui, Q.; Morokuma, K.; Nanayakkara, A.; Challacombe, M.; Malik, D. K.; Rabuk, A. D.; Peng, C. Y.; Ayala, P. Y.; Chen, W.; Wong, M. W.; Andres, J. L.; Replogle, E. S.; Gomperts, R.; Martin, R. L.; Fox, D. J.; Binkley, J. S.; Defrees, D. J.; Baker, J.; Stewart, J. P.; Head-Gordon, M.; Gonzalez, C.; Pople, J. A. *Gaussian 98*, revision A.9; Gaussian Inc.: Pittsburgh, PA, 1998.